The Journal of Engineering

The 14th IET International Conference on AC and DC Power Transmission (ACDC 2018)

IET Journals
The Institution of Engineering and Technology

Real-time optimisation of emergency demand response and HVDC power modulation to improve short-term frequency stability of the receiving-end power systems

eISSN 2051-3305
Received on 28th August 2018
Accepted on 19th September 2018
E-First on 12th December 2018
doi: 10.1049/joe.2018.8682
www.ietdl.org

Luping Wang[1], Xiaorong Xie[1] ✉, Long Peng[2], Yinghong Hu[2], Yuan Zhao[2]

[1]*Department of Electrical Engineering, State Key Laboratory of Power Systems, Tsinghua University, Beijing 100084, People's Republic of China*

[2]*Electric Power Research Institute of State Grid JiBei Electric Power Co., Ltd., Beijing 100045, People's Republic of China*

✉ *E-mail: xiexr@tsinghua.edu.cn*

Abstract: In recent years, large-capacity high-voltage direct currents (HVDCs) have been employed to transfer electricity from the west to the east of China. However, the frequent frequency drops due to HVDC blockings seriously threaten the short-term frequency stability of receiving-end power systems. The existing emergency frequency control strategy is not adaptive to the varying operation conditions and may cause excessive or deficient actions, which could result in inefficient control or high risk of frequency instability. Therefore, a real-time coordinated control strategy is proposed in this study based on the online-updated frequency response model. The model is designed to incorporate multiple types of generators and to reflect the dynamic frequency response of loads. The new control strategy combines multiple control resources, including the emergency demand response and HVDC power modulation, to improve the short-term frequency stability after HVDC failures. By online data preparation and cubic fitting, the nadir of the frequency is expressed as an analytic function of the control variables. A real-time optimisation of emergency controls is achieved to improve the short-term frequency dynamics. Case studies show that the proposed scheme is robust to the varying operation conditions and has lower control cost than the existing control strategy.

1 Introduction

Recently, the HVDC blocking accidents have been happening frequently, threatening the short-term frequency stability (STFS) of large receiving-end power systems such as east China power grid (ECPG) [1]. Early in 2005, Longzheng bipolar HVDC blocking caused the system frequency drop to 49.54 Hz [2]. Since then, HVDC blockings happened frequently. Just in 2016, there occurred 12 HVDC blockings or emergency outages, 4 of which caused large power losses. Among them, the bipolar blocking of Jinsu UHVDC line caused 4.9 GW power loss and a frequency drop of 0.54 Hz. Unfortunately, the STFS problem is becoming worse because of the increasing portion of external power and renewable energy. It reduces the equivalent inertia and frequency regulation capability of receiving-end gird and makes the grid more vulnerable to power disturbances.

Currently, under frequency load shedding (UFLS) is widely used to counter the STFS problem [3]. However, its tripping frequency settings are selected for some specific emergency situations, and therefore not suitable for all cases. The inherent time delays of UFLS relays are too long (up to several seconds) to intercept the frequency decline timely after large disturbances, and must be compensated by conservative margin [4]. Due to the above drawbacks, the trigger of UFLS would generally cause plenty of unnecessary load loss. To solve the problem, the adaptive UFLS (AUFLS) has been widely studied [5]. It uses centralised control, which calculates the amount of load to shed in real time and cuts off the load with small time delay. Compared with conventional UFLS, AUFLS enhances the adaptability and efficiency of the frequency control. However, the accuracy of it is still doubtable because the single-machine system frequency response (SFR) model used in the existing research [3–7] only represents the primary frequency regulation (PFR) characteristics of simplified reheat units and the static frequency response of the load, ignoring the characteristics of different types of generators such as hydro turbines and the dynamic load frequency response.

In other hand, load shedding itself has a price and unplanned load shedding would largely influence industrial production and residential life. In recent years, two emerging frequency control measures have offered better choices. One of them is emergency demand response (EDR) [7], which incorporates industrial and (or) domestic loads into centrally controlled EDR programs through contract. When a power disturbance is met, the control center can issue command to cut off selected loads through direct load control. Since the affected loads are contracted in advance, the influence of EDR is less than (A)UFLS. Besides, the variety of EDR programs also offers the potential of optimisation. The other one is HVDC power modulation (HPM), which can promote the power of HVDC lines very quickly and maintained at a higher level for a period to compensate the unbalanced power caused by a system emergency such as the sudden shutdown of neighboring HVDCs [8]. It has lower control cost because it does not shed any load. Actually, EDR and HPM have already been used in the frequency emergency coordination control system (FECCS) in ECPG. However, the offline control strategy, which is currently adopted in FECCS, still uses empirical SFR model and only prepares limited control plans based on several typical operation modes of the grid. Thus there is a great risk of inefficient control or deficient control as the condition of grid varies. The issue is becoming more and more serious since the increasing portion of the renewable energy makes the unit commitment change more rapidly. In such context, improving the adaptability and accuracy of the STFS control has been more and more urgent.

To solve the problem, a real-time optimised frequency control strategy is proposed in this paper, its features include:

i. The SFR model is extended by taking the PFR characteristics of all types of generators (thermal, nuclear, hydro, and converter-based renewable) and the dynamic loads' frequency response into consideration. The model can be updated online with the change of the operation conditions of power grid.
ii. The nadir of the frequency response is formulated as a cubic function of the control amounts of HPM and EDR by online curve fitting. Thus the optimisation of frequency control measures can be achieved in a real-time way.

iii. It is validated by test examples that the proposed real-time control has better adaptability and control accuracy compared with the offline control.

The rest of the paper is organised as follows: Section 2 describes the target system (ECPG) and the SFR model. Section 3 formulates the optimal control problem and the functional relationship between frequency nadir and control amounts. In Section 4, the implementation of the controls based on real-time optimisation and offline decision-making is discussed. Case studies are carried out in Section 5 and final conclusions are briefed in Section 6.

2 System modelling

2.1 Description of ECPG

ECPG covers five provinces (or municipality): Shanghai, Jiangsu, Zhejiang, Anhui, and Fujian. It is tightly interconnected by over five hundred 500 kV AC transmission lines and thirteen 1000-kV AC transmission lines. Until now, ECPG has seven feed-in HVDC lines. Four of them are 500 kV HVDC lines and each is rated at 3 GW. The other three are 800 kV ultra HVDC (UHVDC), namely Fufeng, Binjin, and Jinsu, with the transmission capacity of 6.4, 8, and 7.2 GW.

The majority of generators in ECPG are thermal units (including nuclear units) and hydro units, with the installed capacity ratio of 85.6 and 9% respectively. The installed wind power and photovoltaic units account for 5.4% [9]. However, because of the priority of renewable energy consumption [10], the proportion of the online capacity of renewable energy units is much higher than the installed capacity. In the near future, the renewable energy generation will continue to increase, but the fluctuation and uncertainty bring a lot of risk to the operation of grid.

To address the STFS problems, in 2016, the FECCS of ECPG was put into operation. It is consisted of a control center, eight HVDC HPM substations, and two EDR programs. The transmission power of HVDC lines can be boosted to 1.1 p.u. of the rated value. All the loads contracted in EDR programs are centrally controlled and can be cut off in <1 s after receiving orders. One of the programs involves up to 9.3 GW water pumping units (EDR 1), and the other includes 1 GW aggregated interruptible load (EDR 2) [11].

2.2 Single bus model

As ECPG is tightly interconnected by high-voltage power lines, the frequency at different places is almost the same. Therefore, the grid can be represented by the widely used single-bus model [3–7, 12]. In the model, (U)HVDC lines, different types of generators, and loads are connected to the same bus as shown in Fig. 1. All (U)HVDC lines except the blocked ones are equipped with HPM function to modulate the transmitted power. According to PFR characteristics, generators in the grid are categorised into three categories: thermal generators (including nuclear units), hydro generators, and converter-based renewable generators. Part of the loads are contracted in EDR programs and can be cut off when needed.

2.3 SFR model

The overall SFR model is illustrated by Fig. 2. Unlike the conventional single-machine model, the proposed model uses real units (except that the frequency deviation Δf is in per unit) and incorporates the PFR model of multiple generator types and the dynamic characteristics of load response. Detailed deduction and explanation of the proposed SFR model are as follows:

i. *Inertia*: System inertia is originated from the rotor inertia of generators. However, for converter-based renewable energy units, the output power is not inherently coupled to the system frequency [13]. Therefore, we only consider the conventional units. Noticing the types of generators are limited, we deduce that

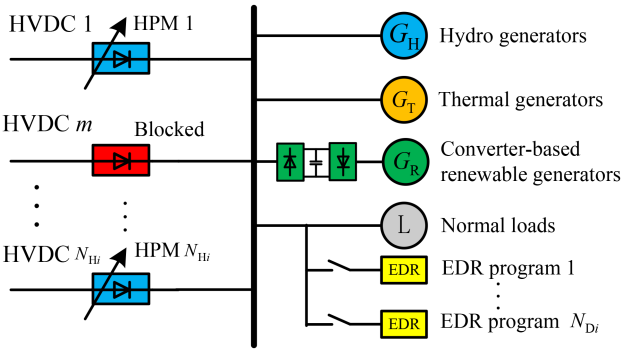

Fig. 1 *Single bus model of ECPG*

$$H \cdot \mathrm{MVA} = \sum_{i=1}^{M_\mathrm{I}} H_i S_i + \sum_{i=1}^{M_\mathrm{J}} H_j S_j \tag{1}$$

where $H \cdot \mathrm{MVA}$ is the equivalent system inertia in real unit [14]; H_i and H_j are the inertial constant of the ith type of thermal unit and the jth type of hydro unit in per unit; M_I and M_J are the number of the types of thermal units and hydro units; S_i is the online capacity of the ith type of thermal unit and S_j is that of the jth type of hydro unit.

ii. *PFR model of generators*: In China, the renewable energy units operate in the maximum power tracking mode [10]. So we only consider the PFR of conventional units. Typical PFR models of thermal and hydro units are expressed as follows [15]:

$$G_\mathrm{T}(s) = -\frac{1}{R} \cdot \frac{1}{1+sT_\mathrm{G}} \cdot \frac{1+sF_\mathrm{HP}T_\mathrm{RH}}{(1+sT_\mathrm{CH})(1+sT_\mathrm{RH})} \tag{2}$$

$$G_\mathrm{H}(s) = -\frac{1}{R} \cdot \frac{1}{1+sT_\mathrm{G}} \cdot \frac{1+sT_\mathrm{R}}{1+s(R_\mathrm{T}/R)T_\mathrm{R}} \cdot \frac{1-sT_\mathrm{W}}{1+0.5sT_\mathrm{W}} \tag{3}$$

where T_G is governor time constant, F_HP is the portion of high pressure cylinder power, T_RH is reheat time constant, T_CH is the time constant of main air chamber, T_R is the reset time of hydro turbine governor, R_T is transient frequency coefficient, and T_W is the start-up time of hydro turbine.

Generally speaking, the PFR parameters of the same type are uniformly set. Thus the overall PFR model

$$G_\mathrm{g}(s) = \sum_{i=1}^{M_\mathrm{I}} G_{\mathrm{T}i}(s) S_i p_i + \sum_{j=1}^{M_\mathrm{J}} G_{\mathrm{H}j}(s) S_j p_j \tag{4}$$

where the subscripts i and j represent the ith type of thermal unit and the jth type of hydro unit. Noticing that part of the units are not able to increase the output power after the contingency [2], we use p_i and p_j to denote the proportion of the units that can provide PFR.

iii. *Dynamic load model*: Based on the frequency response characteristics, the loads can also be divided into three types: type 1 is not directly relevant to system frequency (such as constant power load); type 2 is linear with frequency (like magnetic induction heater etc.); type 3 is induction motor load, the increment of which lags the change of frequency because of rotor inertia. Therefore, the dynamic global load model proposed in [16] is adopted and rewritten as

$$G_\mathrm{L}(s) = P_\mathrm{LD} \cdot \left(K_{\mathrm{L}1} + \frac{K_{\mathrm{L}2}}{T_\mathrm{L}s+1}\right) \tag{5}$$

where P_LD is the total load at time of disturbance, $K_{\mathrm{L}1}$ and $K_{\mathrm{L}2}$ are load parameters, and T_L is the inertia time constant of the type 3 load.

2.4 Modelling control measures

Currently, there are two control measures in the FECCS: namely EDR and HPM. When receiving the control order, selected loads in EDR programs are cut off after a response time. The characteristic is modelled by delayed step function. In other hand, HPM can boost the transmission power from rated power to the maximum in a short time (~200 ms) [11]. To simplify the problem, we also use delayed step function to model HPM. Defining ΔP_{HB} to be the magnitude of power loss because of (U)HVDC blocking, and the power disturbance function is expressed as

$$\Delta P_{\mathrm{HB}}(s) = \frac{-\Delta P_{\mathrm{HB}}}{s} \tag{6}$$

Thus the support power from EDR and HPM is expressed as:

$$\Delta P_x(s) = \frac{\Delta P_x}{s} \mathrm{e}^{-s\tau_x} \tag{7}$$

where ΔP_x is the magnitude of the power support from EDR or HPM; the subscript $x = D, H$ stands for EDR or HPM, respectively; τ_x represents the response time.

2.5 Modelling the controlled system

For a controlled system, the overall power disturbance

$$\Delta P = \Delta P_{\mathrm{HB}}(s) + \sum_{i}^{N_x} \Delta P_{xi}(s) \tag{8}$$

where $N_x = N_D + N_H$; N_D and N_H are the number of EDR programs and (U)HVDC lines, respectively.

According to Fig. 2, we can deduce that the frequency deviation of the controlled system is

$$\Delta f = \left(\frac{-\Delta P_{\mathrm{HB}}}{s} + \sum_{i}^{N_x} \frac{\Delta P_{xi}}{s} \mathrm{e}^{-s\tau_{xi}} \right) \cdot G(s) \tag{9}$$

where

$$G(s) = \frac{1}{2(H \cdot \mathrm{MVA})s - G_{\mathrm{g}}(s) - G_{\mathrm{L}}(s)} \tag{10}$$

Defining the unit step response as:

$$u(t) = L^{-1}\left[\frac{1}{s} \cdot G(s) \right] \tag{11}$$

Equation (10) is rewritten as

$$\Delta f = -\Delta P_{\mathrm{HB}} \cdot u(t) + \sum_{i}^{N_x} [\Delta P_{xi} u(t - \tau_{xi})] \tag{12}$$

3 Optimisation problem

In this paper, the goal of the optimisation is to reduce control cost under the premise of restraining the frequency deviation within the stable constraint. Obviously, the support power from EDR and HPM ΔP_{xi} are the control variables, which cannot exceed the corresponding control capacity. Mathematically, the optimisation problem is formulated as

$$\begin{aligned} &\min \sum_{i=1}^{N_x} c_i \Delta P_{xi} \\ &s.t. \begin{cases} \Delta f_{\mathrm{nadir}} \geq \Delta f_{\mathrm{T}} \\ 0 \leq \Delta P_{xi} \leq \overline{\Delta P_{xi}}, \quad i = 1, 2, \ldots, N_x \end{cases} \end{aligned} \tag{13}$$

where c_i is the normalised control cost; $\Delta f_{\mathrm{nadir}} = \min [\Delta f(t)]$; Δf_{T} is the threshold of frequency deviation for STFS; and $\overline{\Delta P_{xi}}$ is the maximum support power.

The key to solve the optimisation problem (13) is to deduce the relationship between control variables and $\Delta f_{\mathrm{nadir}}$. However, because of the high order of $G(s)$, $\Delta f_{\mathrm{nadir}}$ cannot be analytically solved. Therefore, we use polynomial fitting to get the approximate function $\hat{u}(t)$. Then the approximate $\Delta f_{\mathrm{nadir}}$ (denoted as $\Delta \hat{f}_{\mathrm{nadir}}$) is deduced by solving $\hat{u}(t)$, and the constraint $\Delta f_{\mathrm{nadir}} \geq \Delta f_{\mathrm{T}}$ is substituted by

$$\Delta \hat{f}_{\mathrm{nadir}} \geq \Delta f_{\mathrm{T}} \tag{14}$$

Or the actual optimisation problem to solve in real time is

$$\begin{aligned} &\min \boldsymbol{C}_x \boldsymbol{P}_x \\ &\text{s.t. (14) and } 0 \leq \boldsymbol{P}_x \leq \overline{\boldsymbol{P}}_x \end{aligned} \tag{15}$$

with

$$\begin{cases} \boldsymbol{C}_x = [c_1, c_2, \ldots, c_{N_x}] \\ \overline{\boldsymbol{P}}_x = [\Delta \overline{P}_{x1}, \Delta \overline{P}_{x2}, \ldots, \Delta \overline{P}_{x,N_x}]^{\mathrm{T}} \end{cases} \tag{16}$$

To simplify the fitted function, we select the time interval around the peak of $u(t)$ as is shown in Fig. 3. For a given system, the time values of t_1 and t_2 can be properly selected to make $\Delta f_{\mathrm{nadir}}$ always falls into the interval of (t_1, t_2).

Through extensive calculation, it is found that the performance of cubic fitting is good enough, so we have

$$u(t) \simeq \hat{u}(t) = \sum_{n=0}^{3} p_n t^n, \quad t \in (t_1, t_2) \tag{17}$$

Substitute $u(t)$ with $\hat{u}(t)$ in (12), we have

$$\Delta f(t) \simeq \sum_{n=0}^{3} \beta_n t^n, \quad t \in (t_1, t_2) \tag{18}$$

where

$$\begin{cases} \beta_0 = -P_{\mathrm{HB}} p_0 + \sum_{i=1}^{N_x} \left(P_{xi} \sum_{n=0}^{3} p_n (-\tau_{xi})^n \right) \\ \beta_1 = -P_{\mathrm{HB}} p_1 + \sum_{i=1}^{N_x} \left(P_{xi} \sum_{n=1}^{3} n p_n (-\tau_{xi})^{n-1} \right) \\ \beta_2 = -P_{\mathrm{HB}} p_2 + \sum_{i=1}^{N_x} (P_{xi}(p_2 - 3p_3\tau_{xi})) \\ \beta_3 = p_3 \left(-P_{\mathrm{HB}} + \sum_{i=1}^{N_x} P_{xi} \right) \end{cases} \tag{19}$$

Thus, $\Delta \hat{f}_{\mathrm{nadir}}$ is given by

$$\Delta \hat{f}_{\mathrm{nadir}} = \min \left\{ \begin{matrix} \beta_0 - \dfrac{\alpha_1^3}{27\beta_3^2} - \dfrac{\beta_1 \alpha_1}{3\beta_3} + \dfrac{\beta_2 \alpha_1^2}{9\beta_3^2} \\ \beta_0 - \dfrac{\alpha_2^3}{27\beta_3^2} - \dfrac{\beta_1 \alpha_2}{3\beta_3} + \dfrac{\beta_2 \alpha_2^2}{9\beta_3^2} \end{matrix} \right\} \tag{20}$$

where

$$\begin{cases} \alpha_1 = \beta_2 + \sqrt{\beta_2^2 - 3\beta_1\beta_3} \\ \alpha_2 = \beta_2 - \sqrt{\beta_2^2 - 3\beta_1\beta_3} \end{cases} \tag{21}$$

4 Implementation of real-time control and offline control

4.1 Real-time control process

The process of real-time control is illustrated in Fig. 4*a*, which can be divided into two independent phases, namely online model updating and real-time control optimisation. The detailed procedures are as follows:

i. During normal operation, the SFR model is constantly updated by collecting the breaker status and output power of each generator along with the total load through WAMS/EMS. The parameters of the PFR models of each unit are prepared in advance by regular testing or curve fitting [17]. Inertial constants are gathered from manufactures or previous test. Load model parameters are fitted using recorded data during former contingencies. In the same time, vector $\boldsymbol{C}_x$ and $\overline{\boldsymbol{P}_x}$ are also updated online.

ii. Solve function $u(t)$ with the updated SFR model and obtain $\hat{u}(t)$ by curve fitting. Solve $\Delta\hat{f}_{\text{nadir}}$ to be a function of the control variables.

iii. If there occurs a contingency, the control center would receive the magnitude of disturbance ΔP_{HB}, and solve the optimisation problem (15) in real time. If $\boldsymbol{P}_x = 0$, it means the frequency can remain stable without additional control from FECCS, and thus EDR and HPM will not be triggered. Otherwise, there is no STFS problem, and the control order $\boldsymbol{P}_x$ will be sent to the control terminals so that the control is fulfilled.

4.2 offline control process

Currently, the existing control strategy of FECCS is offline control as shown in Fig. 4*b*. It can be divided into two parts: offline threshold calculating and real-time control matching.

In the offline part, simulation models are prepared according to the operation modes of the target grid. Then, during the simulation under every typical operation modes, the power disturbance is adjusted until the frequency deviation is equal to Δf_{T}, and the corresponding threshold of power disturbance, or ΔP_{T} is found [11]. Finally, the control measures are sorted by control cost and their limit $\overline{\boldsymbol{P}_x}$ is stored in the look-up table (LUT) together with the typical operation modes and corresponding ΔP_{T}.

In the real-time part, once a new contingency occurs, the control center will compare the current grid condition with the typical situation and find the most matched operation mode and the corresponding threshold value ΔP_{T}. The matching degree is determined by the deviation of the real-time total load and the capacity of online conventional generators from that of the typical operation modes. If the power disturbance ΔP_{HB} is greater than the P_{T}, the total power support is calculated as

$$\Delta P_{\text{S}} = \Delta P_{\text{HB}} - \Delta P_{\text{T}} + \Delta P_{\text{M}} \tag{22}$$

where ΔP_{M} is the margin to compensate control delays and other uncertainties. Finally, ΔP_{S} is allocated according to the LUT and the command is issued and executed.

4.3 Advantage of the proposed method

The offline control strategy makes decision based on the offline calculated threshold. However, the typical operation modes are limited, which can deviate from the real situation and cause control error. While real-time control strategy can track the change of the grid operation mode and make the control order in real time. Therefore, the proposed method improves the adaptability and accuracy of short-term frequency control.

5 Case studies

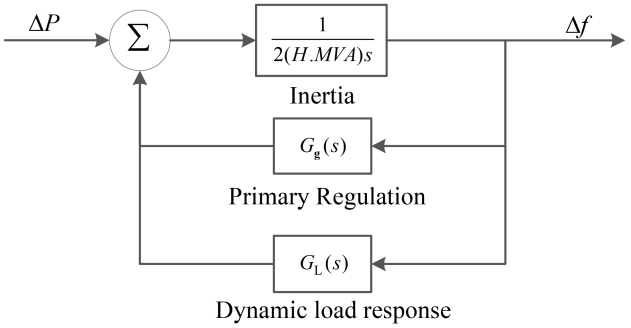

Fig. 2 *Overall SFR model*

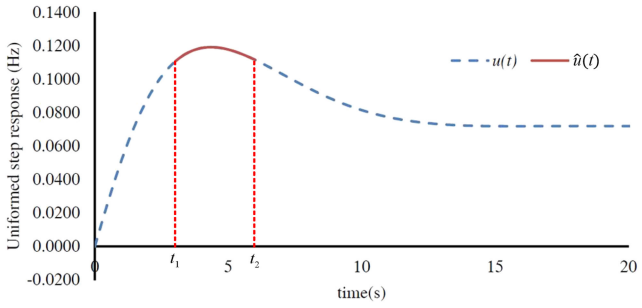

Fig. 3 *Typical curve of u(t) and $\hat{u}(t)$*

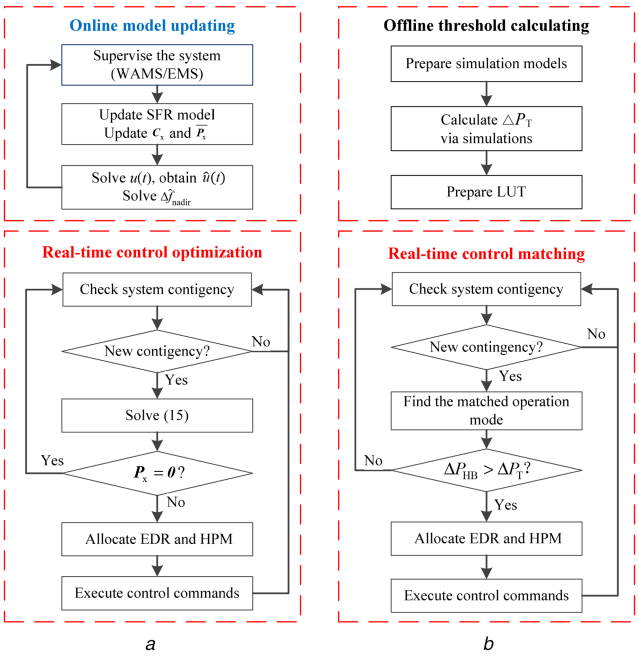

Fig. 4 *Control flow of the two method*
(a) Real-time control, ***(b)*** Offline control

5.1 Studied scenario

We take ECPG as the test grid, and the typical operation mode of autumn flood season is used as the base case [1]. The overall parameters are summarised in Table 1 and the unit is GW (except the proportion). The total load and total capacity of online generators are set according to the operation mode. While the online capacity of hydro units, that of converter-based renewables, and (U)HVDC power are all set to be the rated value. According to the engineering experience in ECPG, generally 50% can provide PFR during large disturbance [2]. The following two cases are studied here:

Case 1: Assuming all the converter-based renewable units are curtailed because of bad weather or other safety issues. The online capacity of thermal units is raised to maintain the required spinning reserve so the total online capacity of generators remains the same.

Case 2: Assuming the proportion of units that can provide PFR is reduced to a half of the former value, or 25%. This situation is possible when the load gets to the peak during the contingency or there are outages of large units.

The Binjin UHVDC has the largest transfer capacity (8 GW) of all (U)HVDCs. A bipolar blocking of it would cause a large disturbance on ECPG. So it is used as the system emergency to test the control strategies. The threshold for STFS or Δf_T is set at −0.5 Hz.

Table 1 Overall parameters of the studied scenario

Parameter	Typical mode	Case 1	Case 2
total load	121	121	121
total capacity of online conventional generators	111	127	111
capacity of online converter-based renewables	16	0	16
capacity of online hydro units	27	27	27
capacity of online thermal units	67	83	67
total (U)HVDC power	33.6	33.6	33.6
proportion of the units that can provide PFR during contingency	50%	50%	25%

Table 2 Parameters of the PFR model of generators

	Thermal units		
Parameter	Type 1	Type 2	Type 3
S	150 MW	300 MW	800 MW
p	20%	30%	50%
R	0.08	0.08	0.08
T_G	0.2 s	0.3 s	0.5 s
T_{RH}	10 s	8 s	7 s
F_{HP}	0.25	0.3	0.5
T_{CH}	0.4 s	0.2 s	0.1 s
H_T	3	5	10

	Hydro units	
Parameter	Type 1	Type 2
S	200 MW	750 MW
p	40%	60%
R	0.08	0.08
T_G	0.2 s	0.4 s
T_R	5 s	10 s
R_T	0.2	0.38
T_W	1 s	2 s
H_H	2 s	5 s

Table 3 Parameters of control measures

Parameter	HPM	EDR 1	EDR 2
c (normalised)	1	2	2.5
τ_x, s [11]	0.2	0.16	0.5
$\Delta\bar{P}_x$, GW	2.56	0.5	1

Table 4 Control schemes and costs

Scenarios	HPM	EDR 1	EDR 2	Normalised cost
	offline control, GW			
case 1 and 2	2.56	0.724	0	4.008
	real-time control, GW			
case 1	2.440	0	0	2.440
case 2	2.560	1	0.612	6.090

In the real practice, the parameters of the generators and load should be updated though periodical test, which need a lot of work. In this paper, we just assume that there are three types of thermal units and two types of hydro units. Table 2 lists the parameters of each type of units, which are selected from the range of value in [15, 18]. The parameters of the dynamic global load model (5) are derived from composite load models widely adopted in Chinese industries [19], which are $K_{L1} = 0.88$, $K_{L2} = 1.32$, and $T_L = 3.0$ s.

Table 3 shows the parameters of the control measures. At present, HPM has the lowest control cost since it does not shed any load. EDR has lower cost than EDR 2 because the former has less influence on daily life and industrial production. The normalised unit control cost is set as shown in Table. 3. The upper limit of HPM is 0.1 p.u. of the rated power for the corresponding line [11]. Considering only part of the pumped storage units are under pumping operation, we assume the upper limit of EDR 1 to be 1 GW.

5.2 Control schemes of the two controls

The key of offline control is to find the most matched operation mode. For the two cases, the total load does not change, and the deviation of the online capacity of conventional generators is quite small. Thus the most matched operation mode is the base case: autumn flood season mode. Through repeated simulation, the threshold ΔP_T is obtained as 4.916 GW. A control margin of 0.2 GW, or $\Delta P_M = 0.2$ GW, is validated in advance to cover the time delays and other uncertainties. Therefore, the total power support from EDR and HPM is 3.284 GW. Taking the ranking of cost into account, the allocation of controls is listed in Table 4.

As for the real-time control, $u(t)$ is updated once the grid condition is changed. So for each case, $u(t)$ is solved and fitted using cubic function. The fitting interval (t_1, t_2) is set to be (4 s, 7 s), and the coefficient of determination R is as high as 0.9999. Then the analytical expression of $\Delta\hat{f}_{nadir}$ is prepared by applying (19)–(21). The control variables are easily solved by interior point algorithm and listed in Table 4.

5.3 Comparison of real-time and offline control

i. *Case 1*: Converter-based renewable energy units are all curtailed: as is shown in Table 4, the real-time control scheme only uses HPM resources and the total control cost is reduced by about 40.2% as compared to that of the offline control. The resulted frequency dynamics as depicted in Fig. 5 shows that the largest frequency deviation under the real-time control is still in the allowable range; while the offline established scheme sheds excessive loads. It is because with the curtailment of renewables, the increased capacity of thermal generators raises the system inertia and the PFR capacity. Thus, during the contingency, less power support is needed. The real-time control formulate the control scheme based on the changed grid condition and therefore reduces the cost.

ii. *Case 2*: The PFR capability is reduced: in this case, it is assumed that the proportion of units providing PFR are reduced to 25%, which is taken into account by the real-time control. Then the real-time control scheme, as shown in Table 4, calls for more power support from EDR. Fig. 6 demonstrates that the frequency is kept above 49.5 Hz by the real-time control. However, the offline control strategy cannot accommodate the offline-made scheme in real time according to system changes. Its controlled frequency goes beyond the threshold. As a result, the regular UFLS would be triggered to trip more loads. In other words, the existing control cannot ensure STFS without the unplanned loss of loads.

The results of the above cases have fully validated that the proposed control strategy is more adaptive and accurate and performs better in maintaining STFS under different system conditions and emergencies than the existing one.

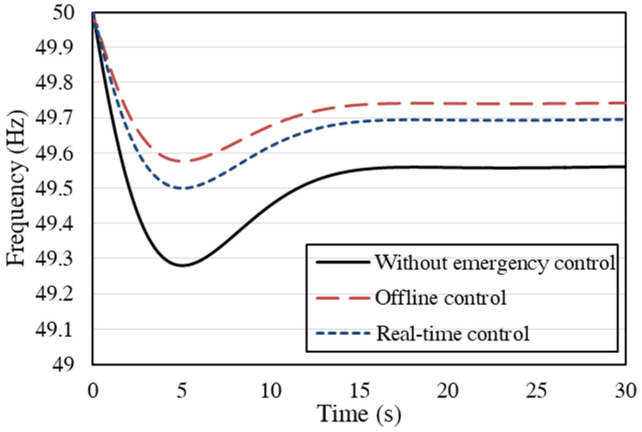

Fig. 5 *Comparison of the control effect of real-time and offline control (case 1)*

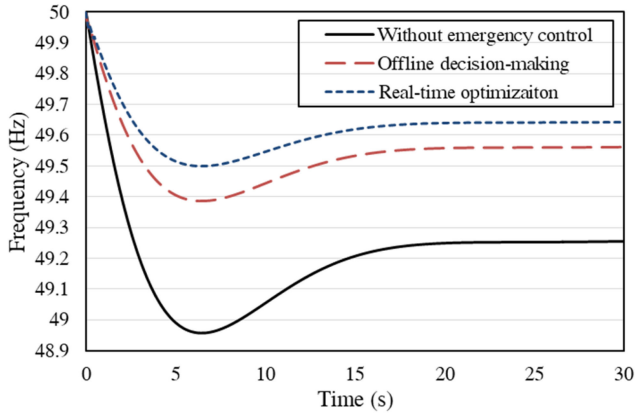

Fig. 6 *Comparison of the control effect of real-time and offline control (case 2)*

6 Conclusion

This paper proposes a real-time optimisation of EDR and HPM in real time to improve STFS for large receiving-end power system. The SFR model is extended by taking multiple types of generators and the dynamic frequency response of load into consideration. Based on the constantly updated SFR model, the curve of the unit step response is prepared online. By cubic fitting, the nadir of frequency deviation is expressed as an analytical function of control variables. Thus the optimisation problem can be solved in real time.

Case studies carried out on ECPG has shown the proposed control strategy is more adaptive and accurate than the existing offline control in maintaining STFS under different system conditions and emergencies. It saves cost by avoiding excessive control in the case curtailed renewables. As the PFR capacity is reduced, the offline control fails to maintain STFS because it cannot accommodate the offline-made control scheme in real time. While the real-time control increases the support power from EDR and successfully maintains the stable of frequency.

7 Acknowledgments

This work is supported in part by National Natural Science Foundation of China (51577097) and State Grid JiBei Electric Power Co., Ltd. (520101170022).

8 References

[1] Li, Z., Wu, X., Wang, L., *et al.*: 'Analysis and reflection on frequency characteristics of east China grid after bipolar locking of '9·19' jinping-sunan DC transmission line', *Autom. Electr. Power Syst.*, 2017, **41**, (07), pp. 149–155

[2] Gao, X., Gao, F., Yang, Z.: 'Frequency accident analysis in east China grid due to DC fault', *Autom. Electr. Power Syst.*, 2006, **30**, (12), pp. 102–107

[3] Anderson, P.M., Mirheydar, M.: 'An adaptive method for setting under frequency load shedding relays', *IEEE Trans. Power Syst.*, 1992, **7**, (2), pp. 647–655

[4] Seyedi, H., Sanaye-Pasand, M.: 'New centralized adaptive load-shedding algorithms to mitigate power system blackouts', *IET Gener. Transm. Distrib.*, 2009, **3**, (1), pp. 99–114

[5] Shekari, T., Aminifar, F., Sanaye-Pasand, M.: 'An analytical adaptive load shedding scheme against severe combinational disturbances', *IEEE Trans. Power Syst.*, 2016, **31**, (5), pp. 4135–4143

[6] You, H., Vittal, V., Yang, Z.: 'Self-healing in power systems: an approach using islanding and rate of frequency decline-based load shedding', *IEEE Trans. Power Syst.*, 2003, **18**, (1), pp. 174–181

[7] Anderson, P.M., Mirheydar, M.: 'A low-order system frequency response model', *IEEE Trans. Power Syst.*, 1990, **5**, (3), pp. 720–729

[8] Harnefors, L., Johansson, N., Zhang, L., *et al.*: 'Interarea oscillation damping using active-power modulation of multi-terminal HVDC transmissions', *IEEE Trans. Power Syst.*, 2014, **29**, (5), pp. 2529–2538

[9] Li, M.: 'East China branch', in Wang, M. (Ed.): '*Yearbook of state grid*' (China Electric Power Press, Beijing, 2016, 1st edn.), p. 228

[10] 'Renewable energy law of the people's republic of China'. Available at http://english.court.gov.cn/2016-04/15/content_24567980.htm, accessed 21 January 2018

[11] Xu, T., Li, G., Zhang, J., *et al.*: 'Design and application of emergency coordination control system for multi-infeed HVDC receiving-end system coping with frequency stability problem', *Autom. Electr. Power Syst.*, 2017, **41**, (08), pp. 98–104

[12] Chang-Chien, L.R., An, L.N., Lin, T.W., *et al.*: 'Incorporating demand response with spinning reserve to realize an adaptive frequency restoration plan for system contingencies', *IEEE Trans. Smart Grid*, 2012, **3**, (3), pp. 1145–1153

[13] Miller, N.W., Clark, K., Shao, M.: 'Frequency responsive wind plant controls: impacts on grid performance'. 2011 IEEE Power and Energy Society General Meeting, San Diego, CA, 2011

[14] Peydayesh, M., Baldick, R.: 'Simplified model of ERCOT frequency response validated and tuned using PMUs data', *IEEE Trans. Smart Grid*, 2017, **PP**, (99), pp. 1–1

[15] Kundur, P.: 'Active power and frequency control', in Balu, J.N. (Ed.): '*Power system stability and control*' (McGraw-hill, New York, 1994, 1st edn.), pp. 581–623

[16] Sullivan, J.W., Malley, M.J.: 'Identification and validation of dynamic global load model parameters for use in power system frequency simulations', *IEEE Trans. Power Syst.*, 1996, **11**, (2), pp. 851–857

[17] Chang-Chien, L.R., Wu, Y.S., Cheng, J.S.: 'Online estimation of system parameters for artificial intelligence applications to load frequency control', *IET Gener. Transm. Distrib.*, 2011, **5**, (8), pp. 895–902

[18] Mircea, E., Mohammad, S.: 'Active power and frequency control', in Anderson, J. (Ed.): '*Handbook of electrical power system dynamics: modeling, stability, and control*' (IEEE Press, Piscataway, 2013, 1st edn.), pp. 291–339

[19] Zhao, L., Li, D., Zhang, W.: 'Simulation research on dynamic load model of north China power grid', *Power Syst. Technol.*, 2007, **31**, (05), pp. 11–16